Supplementary Information for

"High yield production of graphene by liquid phase exfoliation of graphite"

Yenny Hernandez, Valeria Nicolosi, Mustafa Lotya, Fiona M Blighe, Zhenyu Sun, Sukanta De, IT McGovern, Brendan Holland, Michele Byrne, Yurii Gun'ko, John Boland, Peter Niraj, Georg Duesberg, Satheesh Krishnamurthy, Robbie Goodhue, John Hutchison, Vittorio Scardaci, Andrea C. Ferrari, and Jonathan N Coleman*

*colemaj@tcd.ie

S1.0 Experimental

S1.1 Materials

The graphite powder used in the majority of experiments was purchased from Sigma-Aldrich (Product Number 332461) and sieved through a 0.5 mm mesh sieve to remove the larger particles. For some Raman measurements, an additional type of graphite was used. This was in the form of large crystals from Nacional de Grafite, produced by HF dissolution of Graphitic schist, which is a metamorphic, friable rock with large single crystal graphite flakes. Sample preparation was identical for both graphite types. Solvents were obtained from Sigma-Aldrich and used as received.

S1.2 Sample preparation

The graphite was dispersed in the relevant solvent (cylindrical vial, 10-25 ml solvent) at a concentration of 0.1 mg/ml by sonicating in a low power sonic bath (Model Ney Ultrasonic) for 30 minutes. Care must be taken as excessive sonication can lead to destruction of the graphene. The resultant dispersion was then centrifuged (CF) using a Hettich Mikro 22R centrifuge for 90 minutes at 500 rpm. After CF, decantation was carried out by pipetting off the top half of the dispersion. TEM measurements were made by drop casting from the dispersion onto holey carbon grids (400 mesh size). Thin films were prepared by vacuum filtration onto either polyvinylidene fluoride (PVDF) membranes (pore size: 100 nm) or porous alumina membranes (pore size: 20 nm). Initial sample drying was carried out in a vacuum oven at room temperature at a pressure of $\sim 10^{-3}$ mbar. Subsequently, in some cases, annealing was carried out to remove residual solvent using a vacuum tube furnace from GERO Hochtemperaturöfen GmbH. The samples were heated to 400C for 4 hours in either vacuum or forming gas. Samples for AFM were prepared by spraying the graphene dispersions onto silicon dioxide substrates using an Evolution Airbrush (www.graphics.co.uk) spray gun. The solvent was removed by annealing under forming gas at 400 degrees for 4 hours.

S1.3 Equipment and techniques

Absorption measurements were made using a Varian Cary 6000i. Bright and Dark Field TEM images were taken with a Jeol 2100. Some bright field images (figure 3) and associated ED patterns were taken using a Jeol 2010. TEMs were operated at 200 kV in both cases. Atomic force microscopy measurements were made using the DI Multimode from Veeco Systems and the images were obtained under the tapping mode using a 75 kHz tip. X-ray photoelectron spectroscopy was performed using an un-monochromated MgK-alpha X-ray source (photon energy=1253.6 eV) and a CLAM2 analyser manufactured by VG microtech. The base chamber pressure was 2×10^{-10} mbar. Combustion analysis was carried out using a Thermo Deltaplus Continuous Flow Isotope Ratio Mass Spectrometer (CF-IRMS) with

a CE Instruments 1112 Flash elemental analyser interfaced via a Conflo III. Raman spectroscopy was carried out on a Horiba Jobin Yvon LabRAM using a 100X objective lens with a 532 nm laser excitation and a Renishaw MicroRaman spectrometer at 514nm. SEM was carried out using Hitachi S-4300 field emission SEM. Attenuated total reflectance FTIR spectra were taken on a Perkin Elmer Spectrum 100 system.

S1.3.1 Raman spectroscopy: Background

Graphene can be readily identified in terms of number and orientation of the layers by means of elastic and inelastic light scattering, such as Raman [1] and Rayleigh spectroscopies [2,3]. Raman spectroscopy also allows monitoring of doping and defects [3-5].

Raman spectroscopy is a fast and non-destructive method for the characterization of carbons [6]. Their spectra show common features in the 800-2000 cm^{-1} region: the G and D peaks, which lie at around 1560 and 1360 cm^{-1} respectively. The G peak corresponds to the E_{2g} phonon at the Brillouin zone centre. The D peak is due to the breathing modes of sp^2 atoms and requires a defect for its activation [7-9]. It comes from TO phonons around the K point of the Brillouin zone [7,9], is active by double resonance (DR)[8,10] and is strongly dispersive with excitation energy due to a Kohn Anomaly at K[11]. The D peak intensity is not related to the number of graphene layers, but only to the amount of disorder[7,9]. Indeed, when moving from graphite to nanocrystalline graphite, the ratio between the intensity of D and G peak, I(D)/I(G), varies inversely with the size of the crystalline grain[7,9,12].

The 2D peak is the second order of the D peak. This is a single peak in monolayer graphene, whereas it splits in four bands in bi-layer graphene, reflecting the evolution of the band structure[1]. The 2D peak is always seen, even when no D peak is present, since no defects are required for the activation of two phonons with the same momentum, one backscattering from the other. DR can also happen as intra-valley process, i.e. connecting two points belonging to the same cone around the K or K' points. This gives rise to the so-called D' peak, which can be seen around ~1620 cm^{-1} in defected graphite [13].

Defects induce a significant increase of the D and D' intensities, the decrease of the 2D peak height and its broadening, and the appearance of the combination mode around ~2950 cm^{-1}. While all the second order modes in graphene are sums of phonons with the same q, the latter is the combination of the D and D' phonons, and thus requires a defect for its activation.

In defect-free graphene, the variation of Full Width at Half Maximum of the G peak, FWHM(G), is due to doping[3-5]. However, in the case of defected samples, $q \neq 0$ phonons get also activated, resulting in peak broadening [4,7,14].

S1.4 Film formation and structure

Thick films of graphite/graphene were produced by Buchner filtration of the dispersions onto PVDF filter papers. In general, 400 mL of dispersion was filtered to give films weighing 2-4 mg, depending on the dispersion concentration. Such films are typically 5 microns thick. These films could then be used for further analysis, notably optical and electron microscopy and Raman spectroscopy. Note that the position and width of the Raman 2D line shown in figure S1D indicates the presence of graphite rather than graphene [1]. This could be caused by re-aggregation of graphene or by a prevalence of multi-layer flakes.

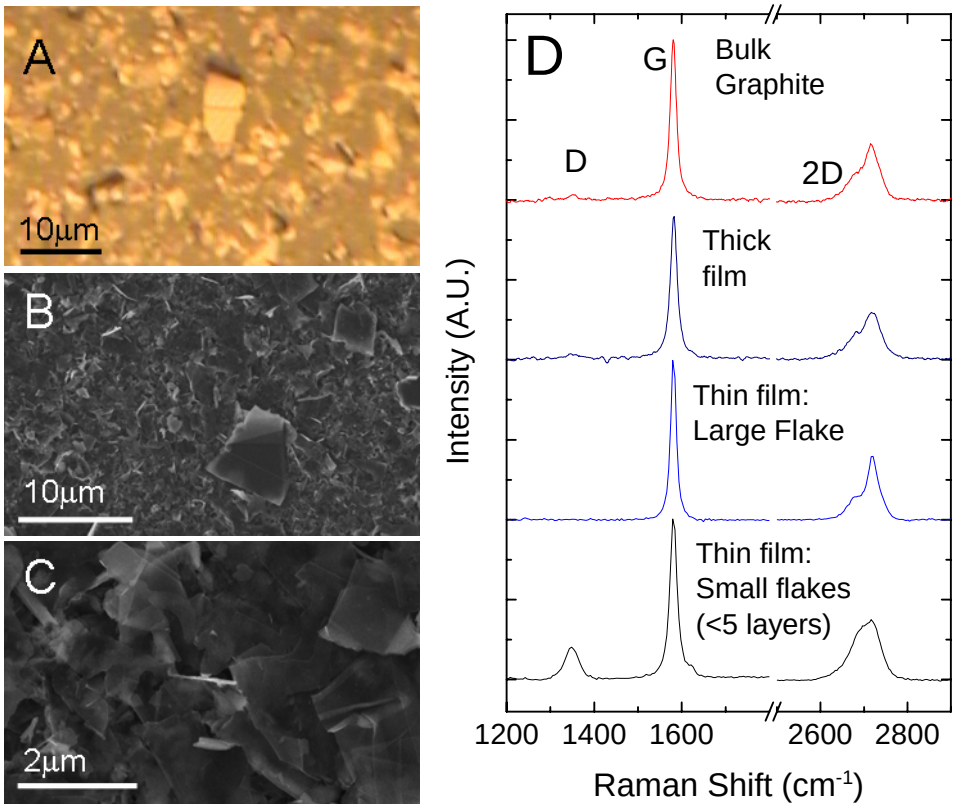

Figure S1 Analysis of the surface of a thin graphene film with a nominal thickness of 30 nm. A) Optical image. B) and C) SEM images. D) Raman spectra for a thick film and a thin film taken by focusing the beam on both large and small flakes. For comparison, spectra taken from bulk graphite and from a vacuum deposited thick film are also shown.

Thin films were prepared by vacuum filtration of dispersions in NMP (0.005mg/ml, 6ml) through porous alumina membranes. These are nominally ~30 nm thick on average as calculated from the mass of material filtered. However, both optical and SEM images indicate that the films consist of random arrays of multilayer flakes. Optical imaging (figure S1A) shows the films to consist of a uniform background

embedded with objects of ~1-10μm in size. SEM imaging (figure S1B) coupled with Raman spectroscopy (figure S1D) point to these large objects being flakes of graphite (ie have more than ~5 layers).

Zooming in on the background region (figure S1C) indicates that the bulk of the material consists of small thin flakes with sizes of ~ 0.5-2 microns. These are very similar to the flakes observed by TEM (see figure 2 and figure S4). Raman spectroscopy shows these flakes to be <5 layers thick (figure S1D). In addition, it should be noted that these films are not totally uniform. It is clear that the mean thickness is significantly larger than the nominal value of 30nm, indicating significant free volume. In addition thickness variations are evident with the membrane occasionally visible.

S2.0 Dispersion quality

S2.1 Best Solvents

The twelve best solvents as characterised by the fraction of graphite/graphene remaining after centrifugation are listed below (also see figure 1). This was calculated by measuring the absorbance after centrifugation and using the measured absorption coefficient, $<\alpha_{660}>=2460$ $Lg^{-1}m^{-1}$, to give the concentration after centrifugation.

Solvent	Surface tension (mJ/m^2)	% remaining after CF	error
Benzyl Benzoate	45.95	8.3	1.1
NMP (1-Methyl-2-pyrrolidinone)	40.1	7.6	1.7
GBL (γ-Butyrolactone)	46.5	7.6	1.7
DMA (N,N-Dimethylacetamide)	36.7	7.2	1.4
DMEU (1,3-Dimethyl-2-Imidazolidinone)	42.5	7.2	1.4
NVP (1-Vinyl-2-pyrrolidone)	42.7	6.6	2.1
N12P (1-Dodecyl-2-pyrrolidinone)	34.5	5.4	1.5
DMF (N,N-Dimethylformamide)	37.1	4.5	1.6
DMSO (dimethyl sulfoxide)	42.98	4.1	1.0
IPA (isopropanol)	21.66	3.4	0.6
N8P (1-Octyl-2-pyrrolidone)	34.5	2.6	2.4
Acetone	25.2	2.5	0.8

Table S1 Best solvents by fraction of graphene/graphite remaining after centrifugation

S2.2 Sedimentation Measurements

Shown in figure S2 is a sedimentation curve measured on a sample that had previously been centrifuged and had the sediment removed by decantation by pouring. We note that the concentration falls over time. This shows that the centrifugation step does not remove all unstable material from the

dispersion. Approximately 28wt% of the dispersed phase sediments out over a period of 3 weeks. This data can be analysed using sedimentation theory[15] (see fit in figure 1) by fitting with a bi-exponential, suggesting the presence of two sedimentation phases and one stable phase[15]. We suggest that the short time-constant (τ_1=1.4 hrs) component represents sedimentation of a very small population of large graphitic flakes which we failed to fully remove when separating the supernatant after centrifugation. (Initial decantation was carried out by pouring which is relatively inefficient. Subsequent decantations were made by taking the top 50% of the centrifuged dispersion). This represents only 4.3wt% of the total mass of graphite/graphene in the sample. The second sedimenting phase represents 22.4wt% of the sample mass and has a much longer time constant (τ_2=152 hrs) indicating much smaller sedimentating objects which we believe to be large flakes of multilayer graphene. Note that there is also a non-sedimenting phase, which consists of the bulk of the sample (71.6wt%). We associate this phase with small graphene monolayers and multilayers.

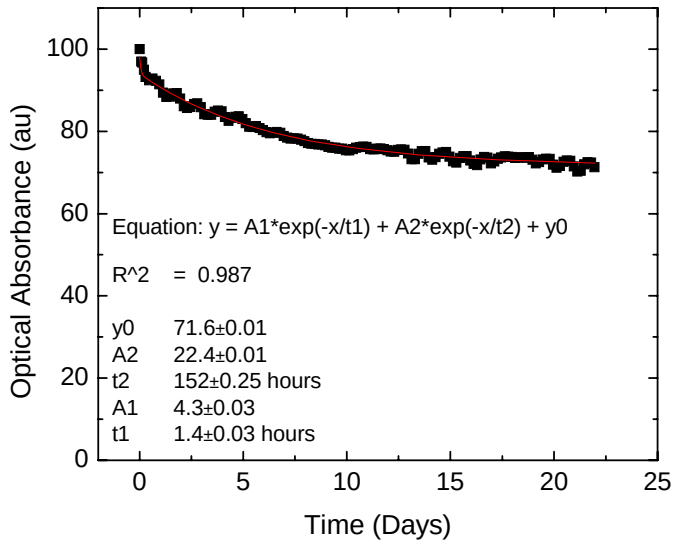

Figure S2 Sedimentation curve for NMP dispersions measured after centrifugation in a home built apparatus[15].

S2.3 HRTEM Statistics

The level of exfoliation of the dispersed material can be characterised using HRTEM, electron diffraction, Raman spectroscopy and atomic force microscopy. Many flakes were observed by HRTEM. Some examples are given in the main text with additional images shown in figure S3. It is possible to count the number of graphene layers per flake for a large number of flakes from these images. These data were calculated for an NMP based sample from images similar to that in figure 2E (TEM grid prepared immediately after centrifugation) and are presented in figure S4 (labelled by t=0). From this we can measure a number fraction of monolayers (number of monolayers / total number of flakes) of 28%. We

can also calculate the mass fraction of graphene, (the mass of monolayer graphene / the mass of all flakes, M_{Ind}/M_T) from:

$$\frac{M_{Ind}}{M_T} = \frac{\sum_{Individuals} A_{monolayer}}{\sum_{Allflakes} N_{monolayer} A_{monolayer}} \qquad \text{Eq S1}$$

where $A_{monolayer}$ is the area of a monolayer and $N_{monolayer}$ represents the number of monolayers in a given flake. The mass fraction was calculated to be 11.8% for the aforementioned NMP based sample. By combining this with the fraction of material remaining after centrifugation (χ, see table S1) we can estimate the total yield of graphene, Y. We define this as the mass of graphene produced divided by the starting mass of graphite: $Y = M_{Ind} / M_T \times \chi$. This gives Y=0.83% for the NMP based sample.

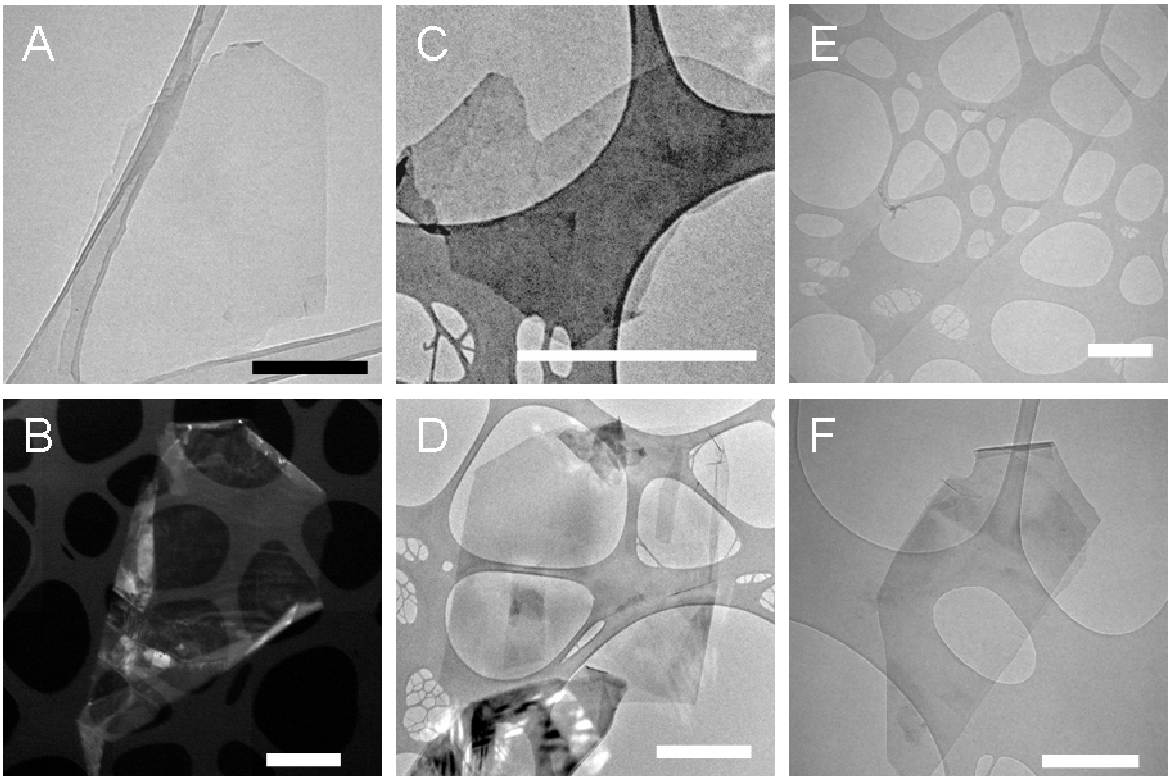

Figure S3 Representative TEM images of monolayer graphene flakes in NMP based samples A) immediately after centrifugation, B) immediately after centrifugation showing scrolling (dark field image), C) four weeks after centrifugation, D) five months after centrifugation, E) and F) prepared by recycling the sediment left over while producing the sample shown in A) and B). E) monolayer F) bilayer. In all cases the scale bar is 500 nm.

S2.4 Stability against re-aggregation

We believe that minimal re-aggregation occurs in the dispersion phase over short timeframes. The vast majority of the flakes observed in the t=0 sample have Bernal stacking. However, we also found two multilayers which showed diffraction patterns with a number of six-fold patterns rotated slightly from

each other, indicative of random stacking[16]. We suggest that we observe Bernal stacking for multilayers which were never exfoliated and random (re)stacking for flakes that did exfoliate but have subsequently re-aggregated in the dispersion phase.

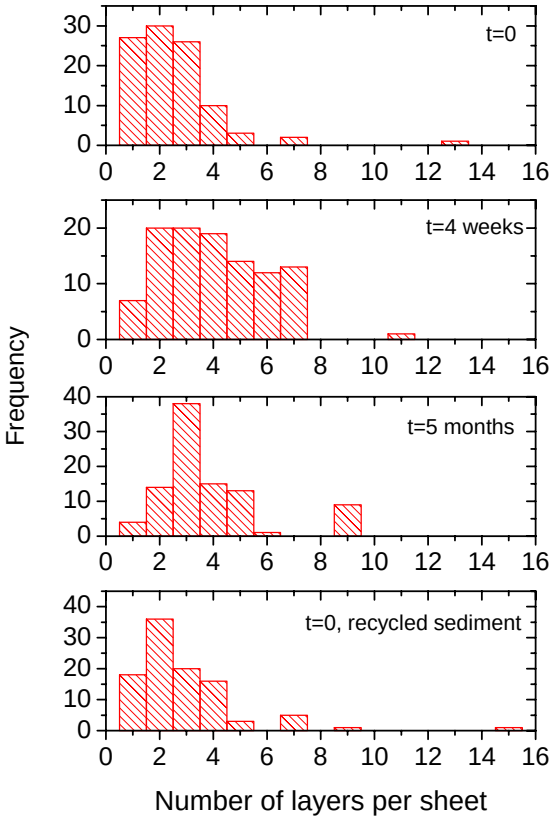

Figure S4 Histograms of the number of graphene layers per flake from samples prepared from NMP based dispersions, immediately after centrifugation and both 4 weeks and 5 months after centrifugation. Statistics are also presented for a sample prepared from re-suspended sediment collected from the original graphene/NMP sample and re-suspended in pure NMP.

We studied re-aggregation over longer timescales by carrying out TEM analysis on dispersions allowed to stand undisturbed for timescales of both 4 weeks and 5 months. Sample images are in figure S3C and D. Shown in figure S4 are histograms of the number of graphene layers per flake for these samples, in comparison to the t=0 sample. For both the 4 weeks and 5 months old samples, we see small but significant amounts of aggregation compared to t=0. This aggregation can be quantified by a decrease in mono-layer number fraction and mass fraction for the aged samples relative to the t=0 sample (table S2). However, both the aged samples contained individual monolayers, demonstrating a reasonable degree of stability. It should be noted that the ensuing aggregation can be reversed at any time by mild sonication. It should be pointed out that it is not clear what happens to the adsorbed NMP after aggregation. However, as aggregation is reversible, we suggest the NMP becomes trapped between the aggregated sheets.

	Number of flakes imaged	Number of mono-layers	Number of multi-layers	Large graphitic objects	Mono-layer number fraction	Mass fraction graphene (M_{Ind}/M_T)	Fraction of material remaining after CF (χ)	Overall yield of graphene: $Y=(M_{Ind}/M_T)\times\chi$
NMP, t=0	100	27	73	0	27%	11.8%	7%	0.83%
NMP, t=4 weeks	106	7	99	0	6.6%	1.8%	7%	0.13%
NMP, t=5 months	94	4	90	0	4.3%	1.1%	7%	0.08%
NMP, recycled sediment	100	18	82	0	18%	6.7%	7%	0.47%
DMEU, t=0	49	3	46	0	6%	2.1%	6.5%	0.14%
GBL, t=0	47	2	45	0	4%	1.5%	6.9%	0.10%

Table S2 Statistics associated with analysis of the TEM images for samples deposited from NMP based dispersions immediately after centrifugation, four weeks after centrifugation and 5 months after centrifugation. Below this data are statistics calculated for a dispersion prepared by re-dispersing a portion of the sediment from the original NMP based dispersion in fresh NMP. Finally we present statistics relating to the TEM analysis of dispersions based on DMEU and GBL. The second, third and fourth columns give the total number of flakes observed divided into number of monolayers and number of multilayers, respectively. Column five shows that no large graphitic objects were observed in any of the dispersions. Columns six and seven show the number fraction of monolayers (number of monolayers / total number of flakes) and the mass fraction of graphene. Column eight gives the fraction of sample remaining after centrifugation. This data allows the calculation of the overall yield, given in column nine.

S2.5 HRTEM statistics for other solvents

We also carried out TEM studies on dispersions prepared from DMEU and GBL immediately after centrifugation. In both cases mono-layers were found. The mono-layer number densities and mass fractions were calculated as 6% and 2.1% respectively for DMEU and 4% and 1.5% for GBL (Table S2).

S2.6 Recycling of sediment

Critically, we attempted to recycle the sediment separated from the original graphene/NMP sample by centrifugation. To do this we dried the sediment and used it to prepare a new dispersion in fresh NMP, in exactly the same way as the original dispersion was made. After centrifugation, this dispersion was analysed using TEM. A significant number of graphene monolayers were observed in addition to large quantities of multi-layers. An example of an image of such a monolayer is shown in figure S3E with a bilayer shown in figure S3F. A histogram of the number of monolayers per multilayer is shown in figure S4. Analysis of the data presented in the histogram allows the calculation of the number density of monolayers and the mass fraction of monolayer graphene to be 18% and 6.7% respectively. These values are similar to those obtained from the original dispersions. This is an important point as it means that the sediment can be effectively recycled. Thus, the real yield of monolayer graphene is not given by $Y = M_{Ind} / M_T \times \chi$, as described above (0.83%) but is actually much larger with a maximum value given by $Y_{\max} = M_{Ind} / M_T$. This allows us to estimate the maximum yield as between the values of M_{ind}/M_T calculated for the recycled sample and the t=0 sample; ie between 6.7% and 11.8%.

S2.7 AFM of deposited sheets

We deposited our graphene/graphite dispersions onto various substrates by spraying with an airbrush. The advantage of this technique is that it allows deposition onto any surface. In principle, any film thickness can be made, from sub-monolayer to many nanometres thick, by controlling the volume of liquid deposited. (In reality it is difficult to optimise the process). We prepared sub-monolayer films of graphene by spraying 1ml at a nitrogen pressure of 2 bar from a distance of 4-5cm away from the sample. This procedure is generally repeated a second time after drying in an oven at 100 degrees for 15 mins to increase the number of deposited flakes. Residual solvent was removed by annealing under forming gas at 400 degrees for 4 hours prior to AFM measurements.

The amount of deposited material was generally low enough that we observed isolated sheets. However, when spraying from high concentration we also saw aggregated sheets (figure S5A and B). While the majority of sheets were relatively thick: 2-5 nm (figure S5A), we also saw significant numbers of thinner objects, which we identify as monolayers. Such objects are typically 1-2 nm in height (figure S5A, B and C) rather than 0.3 nm, in line with the observations of others[17,18]. However, sometimes we measure objects that have very well defined edges but have larger than expected thickness, even up to 2.6 nm (figure S5D). In the course of this work, we noted that very well defined edges are a signature of monolayers in TEM. In fact, by checking the electron diffraction pattern (see main text) for monolayers identified by their edges shows that edge-identification of monolayers is accurate (within a comparison set

of 49 objects). Thus we suggest that the object in figure 5D is a monolayer. That the thickness is much larger than expected is probably due to a combination of chemical contrast issues and the presence of a residual NMP between the monolayer and the SiO_2 substrate. Note the similarity between the shape and

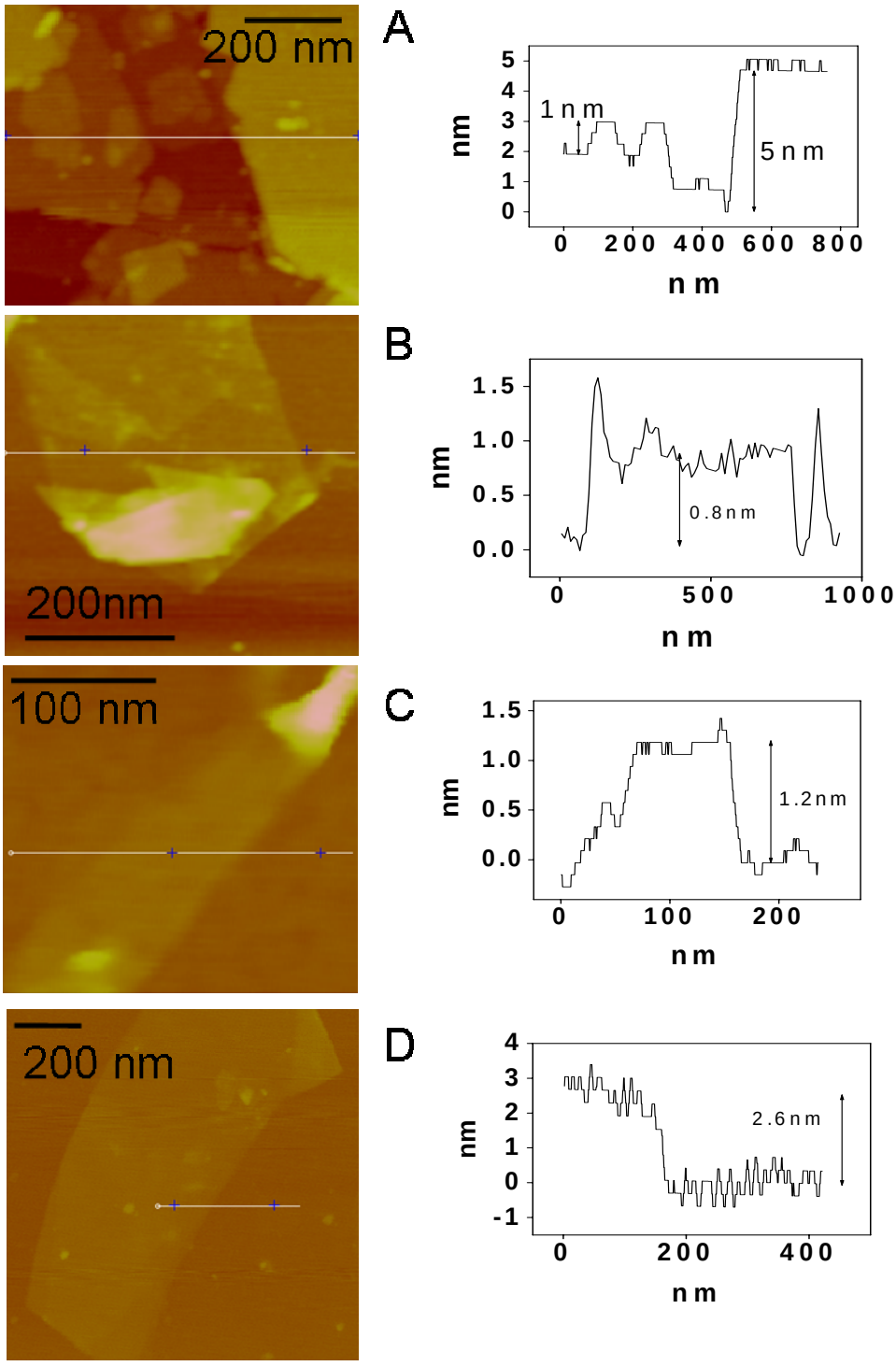

Figure S5 AFM images of a number of flakes observed in this study. The flakes in C) and D) are believed to be monolayers.

size of the graphene sheet in figure S5C and that imaged by TEM in figure S3C (or those in figure 2). This ability to deposit individual sheets is important because it opens up the possibility of preparing samples for electronic applications.

S2.8 Evidence for exfoliation from angle dependent electron diffraction

Further confirmation of the presence of monolayer graphene can be found by measuring the electron diffraction peak intensity as a function of tilt angle. For monolayer graphene, the peak intensity is insensitive to angle while for multi-layer graphene, the intensity can change dramatically with tilt angle[19]. Shown in figures S6A and B are diffraction intensity versus tilt angle data for two flakes identified both visually and from electron diffraction intensity ratios as monolayer and bilayer respectively. As expected the monolayer flake shows angle invariant diffraction intensities while the multilayer shows a collapse of diffracted intensity for the {2110} peaks as the sample holder is tilted to $\pm 10^{o}$. This is further confirmation of the presence of graphene and of our ability to identify it visually.

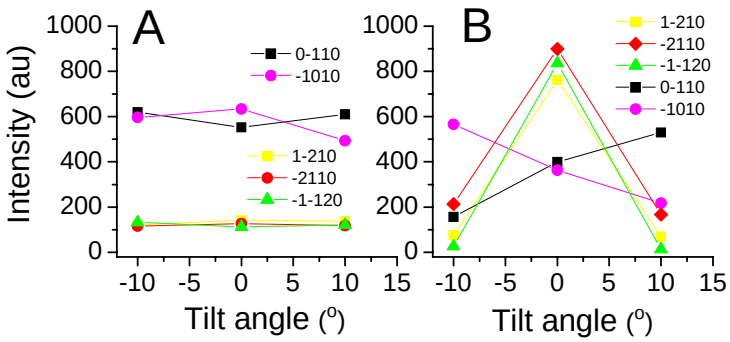

Figure S6 Diffracted intensity for a range of spots as a function of tilt angle for a monolayer (A) and a bilayer (B).

S2.9 Raman spectroscopy I: Exfoliation

Figure S7 plots the Raman spectra for individual flakes deposited from solution onto a marked holey carbon TEM grid (400 mesh). Use of grids as substrates allows us to confirm the nature of the flakes observed in the TEM, and later find the same flake in the Raman spectrometer. These spectra have small or non-existent D bands, indicating an absence of defects. It is possible to identify the number of layers from the shape of the 2D peak[1]. The top spectrum displays a very sharp 2D peak, identifying it as a monolayer. The graphene monolayer studied here is the same one shown in figure 2E and had dimensions of ~1μm. This small size makes these monolayers difficult to find, even on a marked TEM grid. To avoid these difficulties, we used larger sheets (Nacional de Grafite) for the Raman single sheet studies. Subsequent Raman spectra refer to such sheets which are tens of microns in size. The second spectrum has a 2D band shape typical of graphene bilayers. The third can be identified from the 2D band as a graphene

multilayer with less than 5 layers. A spectrum for bulk graphite is shown for comparison. The fact that monolayers, bi-layers and multi-layers (<5 layers) can be detected, confirms again that our method can successfully exfoliate bulk graphite.

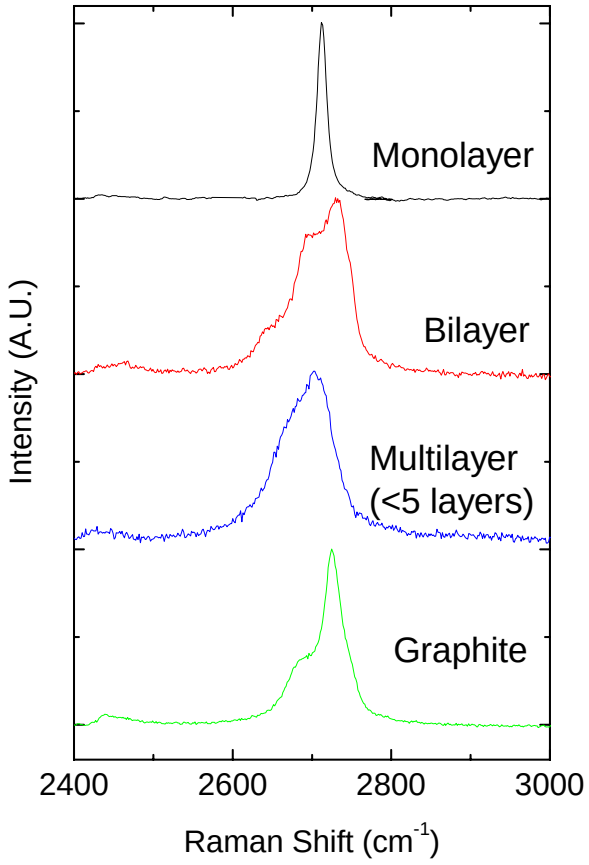

Figure S7. 2D Raman spectra for individual flakes deposited from dispersion on a marked holey carbon TEM grid (400 mesh). The shape of the 2D peak allows identification of the number of layers per sheet. The top spectrum is for a graphene monolayer while the second represents a graphene bilayer. The third can be identified as a graphene multilayer (<5 layers). A spectrum for bulk graphite is shown for comparison. The graphene monolayer studied here is the same one shown in figure 2E (main text).

We also note the shape of the Raman spectrum collected by focussing the laser spot on the region of the thin films characterised by small flakes (figure S1D). The shape of the 2D band is indicative of thin multilayers (<5 layers). This is an important observation as it indicates that very little aggregation occurs in the film formation stage. We note that Eda et al observed monolayers in their graphene oxide films[17]. However, their films were very thin (<2nm) resulting in less opportunity for aggregation in the film formation phase. In addition, as graphene oxide, their flakes were effectively charged[20] which would minimise aggregation. We point out that we prepare films from dispersions of monolayer and multilayer *graphene* not graphene oxide. Our flakes are therefore uncharged and so the lack of large scale

aggregation is pleasantly surprising. However this lack of aggregation is balanced by the presence of residual NMP adsorbed to the flakes (see below).

S3.0 Defects / Purity

The value of this paper is that it demonstrates a method to produce graphene with high yield in the liquid phase. It is important to note that the liquid phase production of graphene oxide (GO) is already well established[17,18,20-22]. However, while reduction of GO can remove some of the oxygen, Raman spectroscopy shows that a large amount of structural defects remain.[17,22] The presence of these defects alters the electronic properties relative to pristine graphene, strongly suppressing the π electrons delocalisation, and massively decreasing the mobility[17]. Thus, to be best of our knowledge, no work to date has shown the exfoliation and dispersion of "pristine" monolayers, bilayers and few layers graphene. It is then critical to further validate that we are not producing graphene oxide or a related version of derivatised graphene. We do this by a combination of X-ray photoelectron spectroscopy (XPS) and attenuated total reflection Fourier transform infrared spectroscopy (ATR-FTIR). In addition we must demonstrate that we are not generating structural defects during the graphene preparation process. This we do through Raman spectroscopy.

S3.1 Raman spectroscopy II: Defect Characterisation

Raman spectra were recorded for thick (~5μm) films deposited from dispersions based on the solvents NMP, GBL and DMEU, as shown in Fig S8. In addition a spectrum for a thin (~30nm) film deposited from NMP is shown. The spectra recorded for thick films are very similar for all solvents and very similar to that of bulk graphite (shown in figure S8 for comparison). This indicates that these films are dominated by flakes greater than 5 layers thick.

In contrast, both large flakes (~10μm) and small flakes are observed in SEM images of the surface of thin films, as described in section S1.4. The Raman spectrum of one of these large flakes is also shown in figure S8 for comparison. Similar to the thick films, the 2D peak is characteristic of graphite showing that these large flakes have >5 layers.

One property common to all the spectra shown in figure S8 is that the D, D' and D+D' lines are virtually invisible, indicating very small amounts of structural defects[1]. We can use this to infer that no inadvertent derivatisation of the graphene/graphite occurrs during the dispersion process. Our results totally contrast the case of graphene oxide[22], where a very large D peak is generally observed[17,21].

It is important to note that, as shown in figure S1D, a small D band is always present in the spectra of films of small flakes. However, this is not surprising. The small flakes are 0.5-2 μm in diameter. As the

laser spot size is 1-2 μm, there will always be a large quantity of edges seen by the beam. These act as defects and are expected to give a D band of similar width to that observed here[1]. The lack of broadening of the G peak also confirms that the D peak comes from edges and not from diffuse structural disorder in the samples. In addition, as mentioned in section S2.9.2, the spectra observed for individual monolayer and multilayers have only small or non-existent D bands, indicating very low defect levels. This is a very important indicator that the monolayers and bi-layers produced here are truly graphene rather than graphene oxide or other forms of derivatised graphene. Taken together with the data for films, this is very strong evidence that the dispersion process does not introduce defects to the basal plane of the graphene.

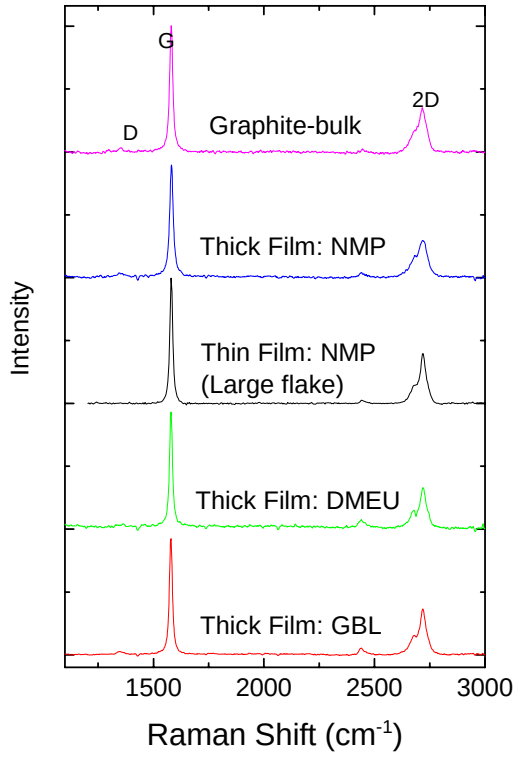

Figure S8 Raman spectra taken for graphite/graphene films. The top is untreated graphite powder. The next two spectra are for thick and thin films respectively of graphene/graphite flakes deposited from NMP by vacuum filtration onto PVDF filter papers. The bottom two are thick films deposited from DMEU and GBL, respectively.

S3.2 X-ray photoelectron spectroscopy

X-ray photoelectron spectroscopy (XPS) was carried out on thin (~30 nm) vacuum filtered films that had been vacuum dried (10^{-3} mbar) at room temperature. Measurements were done on both the as-prepared films (to be referred to as un-annealed) and on a film that was subsequently heated in a tube furnace in vacuum (10^{-3} mbar) to 400C for four hours, to try and remove residual NMP (to be referred to as annealed). Spectra were recorded at 10 eV pass energy and 2 mm slits, with a resolution of 0.85 eV.

XPS spectra were recorded for the un-annealed sample before and after *in vacuo* heating at 600°C to remove atmospheric adsorbates such as CO_2, CO, O_2 and N_2. Employing reasonable cross-section and escape depth approximations, nitrogen 1s core level intensities imply nitrogen concentrations of 1.9 atom% and 1.5 atom% before and after *in vacuo* heating. That the change is small, implies that *in vacuo* heating removed adsorbates such as N_2 but leaves the majority of the NMP trapped in the film. We can use the latter value to estimate a residual NMP content of ~11wt%. Similar nitrogen contents were observed for the annealed sample suggesting that heat treatment is inefficient at removing NMP from the interior of these graphene/graphite films.

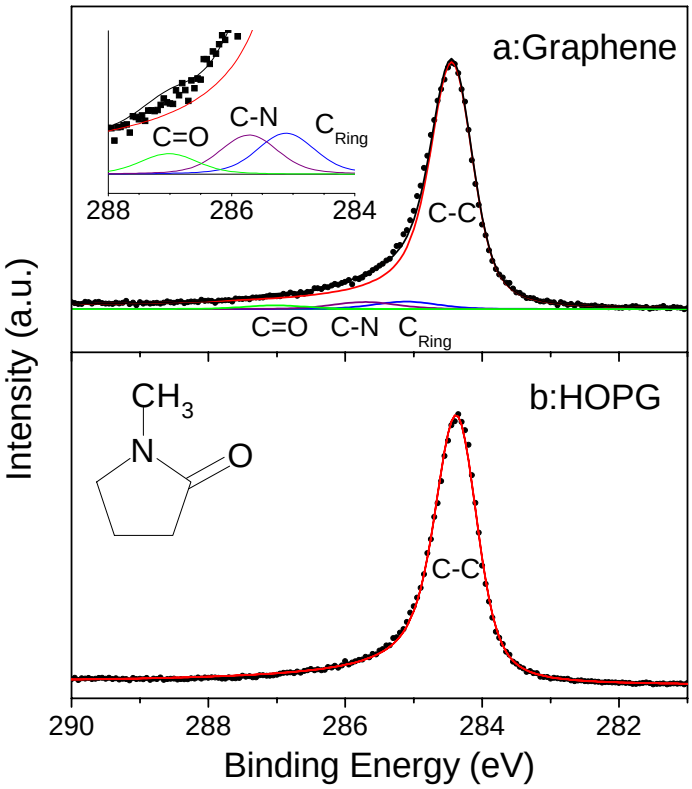

Figure S9 A) XPS spectra for thin (~30 nm) film produced by vacuum filtration of an NMP based dispersion and dried in a vacuum oven at room temperature. Fit lines are labelled as: C-C, graphitic carbon; C_{ring}, Carbon in the NMP ring bonded to two hydrogen atoms; C-N, carbon in the NMP molecule bonded to a N atom; C=O, Carbon in the NMP ring double bonded to an oxygen atom. Inset: a zoomed view of the NMP fit lines. B) XPS spectrum of HOPG. In both cases the Shirley background has been removed. Inset: The structure of NMP.

Carbon 1s core level spectra are shown in figure S9. Spectrum A is from an un-annealed graphene sample which was subjected to *in vacuo* heating at 600°C while spectrum B is from a clean highly-oriented pyrolitic graphite sample (HOPG). Spectrum A has been fitted to the following features:

principally, a HOPG spectrum including a Shirley background and three small Voigt features at 0.7, 1.6 and 2.6 eV higher binding energy than the graphite peak. These features are representative of the two carbon atoms in the NMP ring that are not bonded to N or O, the two carbon atoms that are bonded to N and the carbonyl carbon, respectively. These features have been fit to the spectrum in the intensity ratio 2:2:1, respectively, as would be expected for NMP. For visual clarity the Shirley background has been removed from both spectra. As can be seen, a very good fit is obtained considering only the graphite-like carbon and the NMP carbon (and the Shirley background).

As described above, nitrogen 1s core level intensity implies an estimated 1.5 atom% N in the *in vacuo* heat treated samples. As each NMP nitrogen atom is associated with 5 NMP carbon atoms we can estimate that ~8% of the carbon 1s peak is due to NMP carbons. This compares well with the combined intensity of the remnant (non-graphite-like) features of 7% of the total carbon 1s signal. Thus, this level of solvent residue in graphene provides a reasonable explanation of spectrum A. Both estimates of percentage, however, are individually subject to potential error.

A much firmer conclusion is that there is no discernible trace of graphene oxide in this sample. Similar general conclusions can be drawn for the annealed graphene film. Graphene oxide is generally manifested in XPS by a large C-O peak at 286.2 eV[17,22,23]. Even after reduction and annealing at up to 1100°C, traces of C-O are still observable by XPS[23]. Here no C-O peak is clearly observable. In addition the remnant features around 286 eV can be attributable to residual solvent. Thus, the XPS data strongly suggests that solvent processing does not result in any observable oxidisation of the resultant graphene/graphite. This allows us to confirm that the structures observed by TEM are graphene rather than graphene oxide.

S3.3 ATR-FTIR

Attenuated total reflectance FTIR (ATR-FTIR) spectra were measured for thin films, similar to those shown in figure S1, deposited from NMP dispersions onto alumina membranes by vacuum filtration. The films were dried under vacuum (10^{-3} mbar) at room temperature. One film was subsequently annealed at 400°C for 4 hours in an Ar/H_2 purged atmosphere to remove NMP. The FTIR spectra for both vacuum dried and annealed samples are shown in figure S9 and are virtually featureless. This is in sharp contrast to the spectra for graphene oxide published by Li et. al.[20], which contain intense spectral features around 1700 cm^{-1} attributable to carboxyl groups. Again this is further evidence that we produce graphene rather than some form of derivatised graphene.

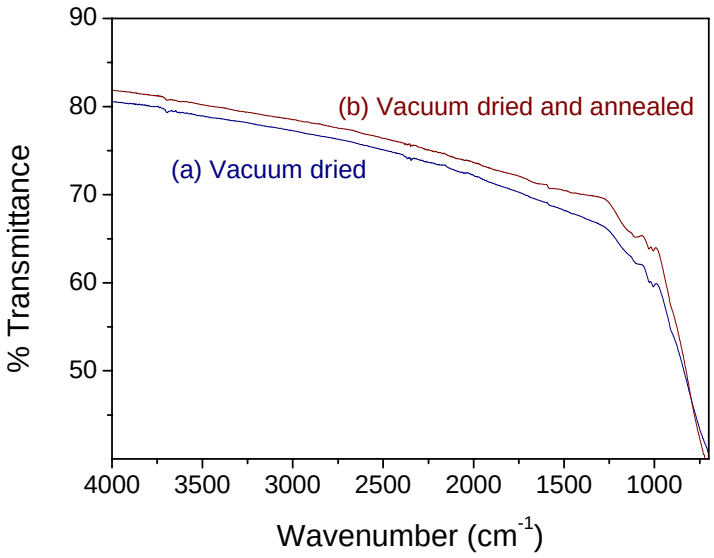

Figure S10 ATR-FTIR spectra for vacuum dried and annealed graphene films. These spectra show no evidence of carboxyl groups which generate features around 1700 cm^{-1}.

S3.4 Presence of residual NMP

NMP is a high boiling solvent which, coupled with the fact that NMP is thought to bind well to graphitic surfaces[24], means that it may be difficult to completely remove NMP from the sample. We have characterised the presence of NMP both for as-prepared samples which have been dried at room temperature under vacuum (10^{-3} mbar)(to be referred to as un-annealed) and on films that were subsequently heated in a tube furnace in vacuum (10^{-3} mbar) to 400C for four hours in an attempt to remove residual NMP (to be referred to as annealed). We have used three techniques to characterise the presence of NMP; XPS, combustion analysis and AFM.

Combustion analysis was carried out on powder recovered from NMP based dispersions using a Thermo Deltaplus Continuous Flow Isotope Ratio Mass Spectrometer (CF-IRMS) with a CE Instruments 1112 Flash elemental analyser interfaced via a Conflo III. Nitrogen was detected at a level of ~1.5 atom% in the un-annealed sample but was not observed in the annealed sample. Taking into account the resolution of the instrument, this means a nitrogen content of <0.9 atom% in the annealed sample. These values correspond to NMP contents by weight of ~11% and <7% respectively.

XPS (see S3.2) was carried out on thin filtered films giving nitrogen contents of ~1.5 atom% before and after annealing corresponding to contents of NMP by weight of ~11%. These results are reasonably close given the different sample types used.

A third, non-quantitative method was also used; AFM. It was found that NMP tends to coalesce into nano-scale puddles on SiO_2. These puddles can be observed by AFM. In the un-annealed sample large quantities of “puddles” are observed. After annealing all puddles are removed. Thus we believe that NMP

is almost totally removed from sub-monolayer films by annealing at 400C for 4 hours. We note however, that the presence of NMP between flakes and substrate (as suggested by AFM) cannot be ruled out.

Technique	N content, un-annealed (atom%)	N content, annealed (atom%)	NMP content, un-annealed wt%	NMP content, annealed wt%
XPS	~1.5	~1.5	~11	~11
Combustion analysis	~1.3	<0.9	~10	<7
AFM	-	-	Large amounts visible	None visible

Table S3 Nitrogen (atom%) and NMP (wt%) contents in both annealed and un-annealed graphite/graphene samples measure using three techniques.

Taken together, these results suggest that NMP cannot be fully removed from thin films or powered samples, with a residual ~10% content. This translates to approximately one NMP molecule per 75 graphene carbons. These molecules are most likely trapped on the internal surface of the powder/film. However, sub-monolayer films have no internal surface, allowing almost complete solvent removal.

S4.0 Thin film conductivity

Thin graphene films were made by vacuum filtration as described above. It proved virtually impossible to remove these films from the alumina membrane so all measurements were made on films on the membranes. All films were approximately 30 nm thick. The sheet resistance of thin films of multilayer graphene were measured by the four-point probe technique. The transparency was measured by comparing the transmitted intensity of a HeNe laser (632nm) through the graphene film on alumina to the transmitted intensity through the alumina alone. Three sample types were prepared. In the first case, after vacuum filtration, the film was dried in a vacuum oven (10^{-3} mbar) at room temperature overnight. This sample had a transmittance of 61% and a sheet resistance of R_s=7.2 MΩ/□. The conductivity of this film was relatively low: ~5 S/m. These results are comparable to that obtained by Eda et al for GO films reduced and annealed (R_s~1 MΩ/□)[17].

Such vacuum dried films were then treated in two ways to improve the conductivity. The first involved heating to 300C in an oven in ambient conditions for 2 hours. This resulted in a slight decrease in transmittance to 42%. However the sheet resistance decreased dramatically to R_s=7.1 kΩ/□. For a thickness of 30 nm this implies a conductivity of 5000 S/m. The second treatment involved annealing in Ar/H_2 (nominally 90%/10%) at 250C for 2 hours. Again the transmittance decreased to 42%. However the sheet resistance dropped dramatically to R_s=5.1 kΩ/□, equivalent to a conductivity of 6500 S/m. This latter value is very close to that observed for films prepared from reduced GO by Li et al (7000 S/m)[20].

It should be noted that these conductivities can almost certainly be improved upon. As shown in figure S1, these films are much thicker than the nominal 30nm. This thickness is that expected if the sheets were close packed. The fact that there is so much free volume means that the number of inter-sheet junctions is much lower than that expected for a dense film. Thus we expect that densification and alignment would result in a significant increase in conductivity as is the case for carbon nanotube films.

S5.0 Composites

Composite dispersions were prepared by adding 3-7g polystyrene to a graphite dispersion in NMP (concentration ~0.01 mg/ml, volume ~400 ml). This was then sonicated for 15 mins in a sonic bath. Composite films were prepared by the film formation method described above. It should be noted that most of the polymer was lost through the filter paper. The graphene/graphite mass fraction was measured by TGA to be in the range 60-85%. At these high volume fractions, the films are very non-uniform as shown in the SEM image in figure S11. Electrical measurements were made by measuring the film resistance as a function of film length. The electrical conductivity of the resultant composite films are shown in figure S12 and range from ~50 S/m for the lowest mass fraction composite to ~700 S/m for the graphene/graphite only film. It is not clear why the conductivity of the graphene/graphite only film deviates from that measured for the thin films. However it is likely to be due to thickness dependent changes in the film morphology.

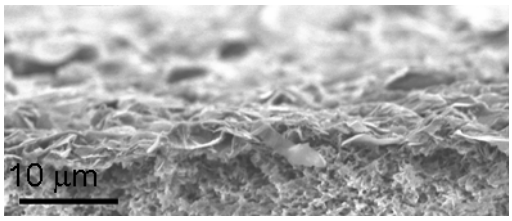

Figure S11 SEM image of the cross section of a polymer-composite film deposited on a PVDF membrane.

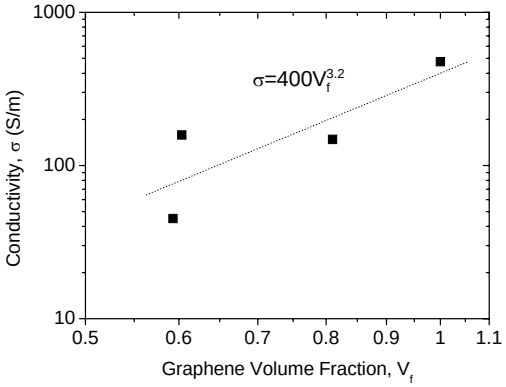

Figure S12 Conductivity of polystyrene composite films prepared by vacuum filtration. The dotted line is a percolation fit with an exponent of 3.2.

S6.0 Calculation of Enthalpy of Mixing

Consider an isolated volume of solvent, V_{sol}, and an isolated mass of graphite, M_G. The graphite can be considered as arranged in flakes of thickness T_1 and area, A_1. The number if such flakes is $N_1 = M_G / \rho_G T_1 A_1$, where ρ_G is the graphite density.

The enthalpy of mixing of solvent and graphite can be found by calculating the energy required to separate all molecules (solvent/graphene sheet) to infinity minus the energy to bring them back together in the form of a solvent-graphite dispersion, but with flakes of different thickness. This can be divided into five energetic components.

1. The energy required to separate all graphene sheets to infinity is given by the energy required to create the surfaces associated with the individual graphene sheets and so is related to the effective graphite surface energy, E_{Sur}^{G}, which can be thought of as the inter-sheet binding energy per unit area of surface.

$$E_1^{NT} = N_1\left[\left(\frac{T_1 A_1}{tA}\right)2A - 2A_1\right]E_{Sur}^{G}\ \text{Eq} \qquad \text{Eq S2}$$

where the term in the round brackets represents the number of graphene sheets per flake and the second term in the square brackets represents a correction for the outer surface of the flake. Here, t and A are the thickness and area of individual graphene sheets.

2. The energy required to remove all the solvent molecules to infinity is given by

$$E_1^{Sol} = V_{sol}E_{Coh}^{Sol} - A_1^{Sol}E_{Sur}^{Sol} \qquad \text{Eq S3}$$

where E_{Coh}^{Sol} is the solvent cohesive energy, E_{Sur}^{Sol} is the solvent surface energy and A_1^{Sol} is the external surface area of the solvent.

3. The energy retrieved by bringing the graphene sheets back from infinity to form N_2 flakes of thickness, T_2, and length, L_2, is similar to E_1^{NT} and is given by

$$E_2^{G} = N_2\left[\left(\frac{T_2 A_2}{tA}\right)2A - 2A_2\right]E_{Sur}^{G} \qquad \text{Eq S4}$$

Where $N_2 = M_G / \rho_G T_2 A_2$

4. We can also calculate the energy released by bringing the solvent molecules back from infinity to form a liquid but leaving voids *to accommodate the reconstituted flakes*:

$$E_2^{Sol} = V_{sol}E_{Coh}^{Sol} - A_2^{Sol}E_{Sur}^{Sol} - A_{Inter}^{G-sol}E_{Sur}^{Sol} \qquad \text{Eq S5}$$

Here A_2^{Sol} is the new solvent (outer) surface area, while A_{Inter}^{NT-sol} is the surface area of the voids, which will accommodate the flakes.

5. Finally we must calculate the interfacial energy associated with placing the flakes in the voids:

$$E_2^{G-Sol} = 2A_{Inter}^{G-Sol}E_{Inter}^{G-Sol} = 2N_2 2A_2 E_{Inter}^{G-Sol} \qquad \text{Eq S6}$$

where E_{Inter}^{G-Sol} is the solvent-graphite binding energy per unit area. The factor of two comes from the fact that we are passivating two surfaces, that of the graphene and that of the solvent.

The enthalpy of mixing is given by

$$\Delta H_{Mix} = E_1^G + E_1^{Sol} - (E_2^G + E_2^{Sol} + E_2^{G-Sol}) \qquad \text{Eq S7}$$

This can be calculated using the expressions outlined above. A number of approximations can be made. One is that the solvent external surface area is the same before and after mixing with the graphite ($A_2^{Sol} \approx A_1^{Sol}$), a reasonable approximation at low graphite content. In addition, we assume that the flakes that exist in the graphite powder are much larger than those in the dispersion ($T_1 >> T_2$). Including these approximations, this works out to be

$$\Delta H_{Mix} \approx 2\frac{M_G}{T_2\rho_G}\left[E_{Sur}^G + E_{Sur}^{Sol} - 2E_{Inter}^{G-Sol}\right] \qquad \text{Eq S8}$$

Finally, we note that the volume fraction of graphite, ϕ, is given by $\phi = M_G / \rho_G V_{Mix}$, where V_{Mix} is the volume of the mixture. Then:

$$\frac{\Delta H_{Mix}}{V_{Mix}} \approx 2\frac{\phi}{T_2}\left[E_{Sur}^G + E_{Sur}^{Sol} - 2E_{Inter}^{G-Sol}\right] \qquad \text{Eq S9}$$

In general, for materials that interact predominately by dispersive interactions we can estimate E_{Inter}^{G-sol} from the geometric mean approximation[25]:

$$E_{Inter}^{G-sol} \approx \left[E_{Sur}^G E_{Sur}^{Sol}\right]^{1/2} \qquad \text{Eq S10}$$

Substituting this in above we get

$$\frac{\Delta H_{Mix}}{V_{Mix}} \approx \frac{2}{T_{flake}}\left(\delta_G - \delta_{sol}\right)^2 \phi \qquad \text{Eq S11}$$

where

$\delta_i = \sqrt{E_{Sur}^i}$ and where we write T_2 as T_{flake} for clarity.

The solvent surface energy, E_{Sur}^{Sol}, is related to the surface tension, γ^i, by [26]:

$$\gamma = E_{Sur}^{Sol} - TS_{Sur}^{Sol} \qquad \text{Eq S12}$$

where S_{Sur}^{Sol} is the solvent surface entropy. The surface entropy is a generic liquid property that tends to have values in the range 0.07-0.14 mJ/m^{2}K. Liquids of a given class tend to have very similar values of S_{Sur}^{Sol}, with DMF and toluene for example shown to have values close to $S_{Sur}^{Sol} = 0.11 mJ/m^2K$ [27]. Thus, we take the universal value to be ~0.1 mJ/m^{2}K and use this to transform between γ and S_{Sur}^{Sol} in figure 1.

References

[1] Ferrari, A. C. et al., Raman spectrum of graphene and graphene layers. *Physical Review Letters* **97** (18) (2006).

[2] Blake, P. et al., Making graphene visible. *Applied Physics Letters* **91** (6) (2007).

[3] Pisana, S. et al., Breakdown of the adiabatic Born-Oppenheimer approximation in graphene. *Nature Materials* **6** (3), 198 (2007).

[4] Casiraghi, C. et al., Raman fingerprint of charged impurities in graphene. *Applied Physics Letters* **91** (23) (2007); Ferrari, A. C., Raman spectroscopy of graphene and graphite: Disorder, electron-phonon coupling, doping and nonadiabatic effects. *Solid State Communications* **143** (1-2), 47 (2007).

[5] Das, A. et al., Monitoring dopants by Raman scattering in an electrochemically top-gated graphene transistor. *Nature Nanotechnology* **3** (4), 210 (2008).

[6] Ferrari, A. C. and Robertson, J., Raman spectroscopy in carbons: from nanotubes to diamond. *Phil. Trans. Roy. Soc. A.* **362**, 2267 (2004).

[7] Ferrari, A. C. and Robertson, J., Interpretation of Raman spectra of disordered and amorphous carbon. *Physical Review B* **61** (20), 14095 (2000).

[8] Thomsen, C. and Reich, S., Doable resonant Raman scattering in graphite. *Physical Review Letters* **85** (24), 5214 (2000).

[9] Tuinstra, F. and Koenig, J. L., RAMAN SPECTRUM OF GRAPHITE. *Journal of Chemical Physics* **53** (3), 1126 (1970).

[10] Baranov, A. V., Bekhterev, A. N., Bobovich, Y. S., and Petrov, V. I., Interpretation of some singularities in raman-spectra of graphite and glass carbon. *Optika I Spektroskopiya* **62** (5), 1036 (1987).

[11] Piscanec, S. et al., Kohn anomalies and electron-phonon interactions in graphite. *Physical Review Letters* **93** (18) (2004).

[12] Knight, D. S. and White, W. B., CHARACTERIZATION OF DIAMOND FILMS BY RAMAN-SPECTROSCOPY. *Journal of Materials Research* **4** (2), 385 (1989).

[13] Nemanich, R. J. and Solin, S. A., 1ST-ORDER AND 2ND-ORDER RAMAN-SCATTERING FROM FINITE-SIZE CRYSTALS OF GRAPHITE. *Physical Review B* **20** (2), 392 (1979).

[14] Ferrari, A. C., Rodil, S. E., and Robertson, J., Interpretation of infrared and Raman spectra of amorphous carbon nitrides. *Physical Review B* **67** (15) (2003).

[15] Nicolosi, V. et al., Solubility of Mo6S4.5I4.5 nanowires in common solvents: A sedimentation study. *Journal of Physical Chemistry B* **109** (15), 7124 (2005).

[16] Horiuchi, S. et al., Single graphene sheet detected in a carbon nanofilm. *Applied Physics Letters* **84** (13), 2403 (2004).

[17] Eda, G., Fanchini, G., and Chhowalla, M., Large-area ultrathin films of reduced graphene oxide as a transparent and felxible electronic material. *Nature Nanotechnology* **3**, 270 (2008).

[18] Stankovich, S. et al., Graphene-based composite materials. *Nature* **442** (7100), 282 (2006).

[19] Meyer, J. C. et al., The structure of suspended graphene sheets. *Nature* **446** (7131), 60 (2007); Meyer, J. C. et al., On the roughness of single- and bi-layer graphene membranes. *Solid State Communications* **143** (1-2), 101 (2007).

[20] Li, D. et al., Processable aqueous dispersions of graphene nanosheets. *Nature Nanotechnology* **3** (2), 101 (2008).

[21] Dikin, D. A. et al., Preparation and characterization of graphene oxide paper. *Nature* **448** (7152), 457 (2007).

[22] Stankovich, S. et al., Synthesis of graphene-based nanosheets via chemical reduction of exfoliated graphite oxide. *Carbon* **45** (7), 1558 (2007).

[23] Becerril, H. A. et al., Evaluation of solution-processed reduced graphene oxide films as transparent conductors. *Acs Nano* **2** (3), 463 (2008).

[24] Bergin, S.D. et al., Towards Solutions of SWNT in Common Solvents. *Advanced Materials* **20** (10), 1876 (2007).

[25] Hildebrand, J.H, Prausnitz, J.M., and Scott, R.L., *Regular and related solutions*, First ed. (Van Nostrand Reinhold Company, New York, 1970); Girifalco, L. A. and Good, R. J., A Theory for the Estimation of Surface and Interfacial Energies .1. Derivation and Application to Interfacial Tension. *Journal of Physical Chemistry* **61** (7), 904 (1957).

[26] Lyklema, J., The surface tension of pure liquids - Thermodynamic components and corresponding states. *Colloids and Surfaces a-Physicochemical and Engineering Aspects* **156** (1-3), 413 (1999).

[27] Tsierkezos, N. G. and Filippou, A. C., Thermodynamic investigation of N,N-dimethylformamide/toluene binary mixtures in the temperature range from 278.15 to 293.15 K. *Journal of Chemical Thermodynamics* **38** (8), 952 (2006).